Experimental investigation of large-scale high-velocity soft-body impact on composite laminates

A D Cochrane, Joël Serra, J K Lander, I K Partridge, H Böhm, T Wollmann, A Hornig, M Gude, S R Hallett

Experimental investigation of large-scale, high strain-rate delamination under soft-body impact

A. D. Cochrane[1], J. Serra[1], J. K. Lander[2], I. K. Partridge[1], H. Böhm[3], T. Wollmann[3], A. Hornig[3], M. Gude[3], and S R Hallett[1]

[1]*Bristol Composites Institute (BCI), University of Bristol, United Kingdom*

[2]*Rolls-Royce plc, United Kingdom*

[2]*Institute of Lightweight Engineering and Polymer Technology (ILK), Technische Universität Dresden, Germany*

Abstract

High-performance aerospace laminated composite structures manufactured from carbon-fibre prepreg are very susceptible to delamination failure under in-flight impact conditions. Much testing has been conducted at small length scales and quasi-static strain-rates to characterise the delamination performance of different material systems and loading scenarios. Testing at this scale and strain-rate is not representative of the failure conditions experienced by a laminate in a real impact event. Full-scale testing has also been conducted, but much of this is not in the open literature due to intellectual property constraints. Testing at this scale is also prohibitively expensive and involves complex failure mechanisms that cause difficulty in the analysis of associated failure behaviour. A novel test is presented which provides a simple, affordable alternative to full-scale testing but which invokes failure at sufficient scale and strain-rate to be representative of real component failure. This test design is experimentally validated through a series of soft-body gelatine impact tests using a light gas-gun facility. A fractographic analysis using scanning-electron microscopy was undertaken to examine microscopic failure behaviour, showing a possible reduction in crack mode-ratio during propagation.

1 Introduction

The use of carbon-fibre reinforced plastic (CFRP) in aerospace structures is now widespread and allows component manufacturers to achieve enhanced and tailored properties while simultaneously reducing weight. CFRP materials are increasingly being deployed in the most high-performance of applications such as in rotating gas-turbine engine components [1]. A major drawback of such materials is that whilst they offer very high stiffness, they are relatively brittle [2]. Energy absorption mechanisms are therefore different from those of more ductile materials such as metals, with a significant example being that of interlaminar crack formation through a process known as delamination. Composite components are particularly susceptible to delamination under impact conditions such as during bird-strike [3, 4]. Delaminations may propagate in a rapid and unstable manner throughout a composite structure and cause significant reductions in residual structural stiffness, leading to potentially catastrophic in-flight events if left unchecked. Composite structures are now being designed and produced to have improved levels of damage tolerance, measurable by the ability of a structure to reduce progressive crack growth and thus improve their resilience to structural failure [5]. A contributing factor to this improved damage tolerance are advances in material technology, such as the inclusion of thermoplastic particles embedded in the matrix resin [6].

The damage tolerance of a carbon fibre pre-preg laminate is defined predominantly by the interlaminar fracture toughness, a property governed by the neat matrix resin which constitutes the interface between the fibrous ply layers. Its strength is substantially lower than that of the fibres, and so is a limiting factor in the impact performance of laminated prepreg-manufactured aerospace structures where there is a lack of fibrous material in the through-thickness direction. The interlaminar fracture toughness of composite laminates is most commonly characterised at coupon level and at quasi-static strain-rates through a series of standard tests representing different loading conditions. The established test types are double-cantilevered beam (DCB) [7] for Mode I, end-loaded split (ELS) [8] and end-notched flexure (ENF) [9] for Mode II and mixed-mode bending (MMB) [10] for mixed-mode. More recently, such tests have been extended to include through-thickness reinforcement (TTR) such as Z-pins to assess reinforced fracture toughness [11], but the modified test methods are not yet formalized in any standard. Fracture toughness tests such as those described generally involve loading specimens of fixed geometry, boundary conditions and loading or displacement extents and rates to benchmark interlaminar properties between different material systems under common circumstances.

The need for a sub-element scale test in which large delaminations are developed is highlighted by the case of

Z-pin TTR, which is used to reinforce the interlaminar regions in laminates made from pre-impregnated material (pre-preg). It has been established that in order to test the efficacy of Z-pin TTR in arresting crack propagation, a Z-pin array must encounter a crack over sufficient distance – and thus be implemented in a structure of sufficient scale – to invoke *large-scale bridging* of that array [11–13]. During large-scale bridging the crack becomes large enough to cause pins to 'bridge' the fracture surfaces over sufficient distance to generate the maximum possible bridging force to suppress further propagation (Figure 1). At the fracture toughness coupon test scales described previously, such large-scale bridging behaviour is not possible. In a full-scale impact event, such as on an aircraft structural component at take-off speed, the delaminations produced will likely be large in scale and occur at high strain-rate. Full-scale industrial gelatine impact testing has been conducted to evaluate the effect of this type of event, but such testing is prohibitively expensive, performed on complex geometry and produces sophisticated failure mechanisms that are difficult to isolate and analyse [14–16]. Data on recent testing at this scale is also not available in the open literature due to intellectual property constraints. A simple, affordable and laboratory-scale test is thus required which yields delamination failure of sufficient scale - in this case described as *large scale* - to invoke large-scale bridging, takes place at high enough strain-rate to be representative, and which uses a specimen of basic geometry which may be readily modelled and simplified for analysis purposes.

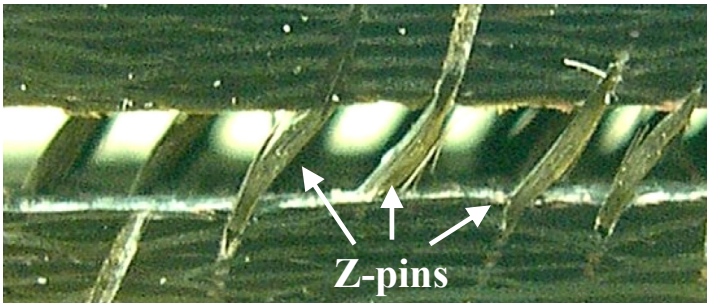

(a)

Figure 1: Mixed-mode crack-bridging by an array of Z-pins through-thickness reinforcement [17];

The closest emulation of high strain-rate, large-scale delamination conditions in a laboratory-scale test has been the Soft-Body Beam-Bending (SBBB) test, which was developed as a representative analogue to reproduce loading conditions observed in a full-scale component under impact but in a much smaller specimen and rig [18] (Figure 2). With high levels of bending allowed under a normal soft-body impact, the intended failure mode was a large primarily Mode II delamination starting from a single pre-crack, inserted at the mid-plane and mid-span of the laminate. The SBBB method is a very relevant example of a test which has been developed to induce a specific type of failure and avoid failures which will negatively affect the test's ability to be representative (i.e. produce delamination without fibre failure). The test parameters used, for example the test velocity range of 100 - 200m/s, have been specifically selected to reproduce loading conditions observed in a real aerospace component

in-flight at take-off and landing forward speeds. The test has been conducted on Z-pinned laminates to investigate the Mode II capability of normally-aligned carbon-fibre Z-pins under soft-body impact [19]. However, it was found that the SBBB test method was still insufficient to produce large-scale bridging in an array of Z-pins. The current study therefore aims to produce a novel test standard which eliminates the described shortcomings.

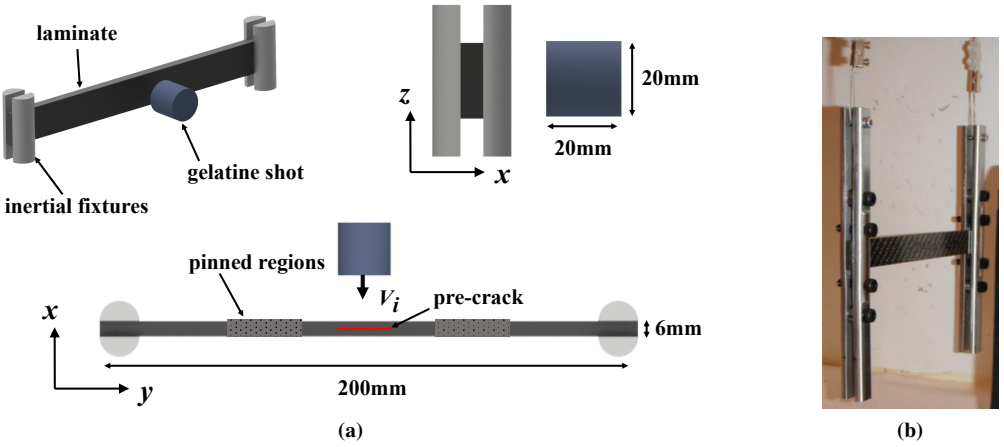

Figure 2: (a) shows an illustration of the test design and geometry for the Soft-Body Beam-Bending (SBBB) test, and (b) shows a photograph of the experimental setup [19]

An example of a larger-scale sub-element type test used to demonstrate the impact damage performance of different materials systems at high velocities was presented by Hou et al [20]. The presented test method is one of the few large sub-element type tests on a composite structure which makes use of soft-body impact, a cantilevered-type test specimen and investigates delamination behaviour at high strain-rate presented in the literature to date. Other studies, such as in [21], have examined impact on cantilevered plates but where the projectile was 'sliced' by the leading edge of the specimen to represent impact of a gas-turbine rotating engine component. For the current study, full surface impact was more suitable to generate greater bending and resulting delaminations, with fewer unknowns and variability, such as slice length. Use of full surface impact also allowed for quantification of the exact amount of kinetic energy transmitted to the plate during testing. In [20], cylindrical gelatine projectiles were fired at composite laminate flat plates of in-plane dimensions $216 \times 102mm$ near the leading edge at the mid-span point and at an angle of 40° to the laminate surface (Fig. 3(a)). The length of laminate which sits under the clamping fixture is notable - which is just over 10% of overall laminate length. The laminates were subjected to impact at speeds between $200m/s$ and $300m/s$, and the gelatine velocity was measured by high-speed camera. The laminate damage was then measured via ultrasonic C-scan after the testing. For some tests, projectile mass was altered by increasing projectile length while maintaining diameter. The research in [20] outlined the ability to change failure modes by altering projectile mass - it was found that larger masses at lower velocities initiated damage from the root (Figure 3(b)) region, while high velocities and small

masses produced local failure near the impact zone (Figure 3(c)).

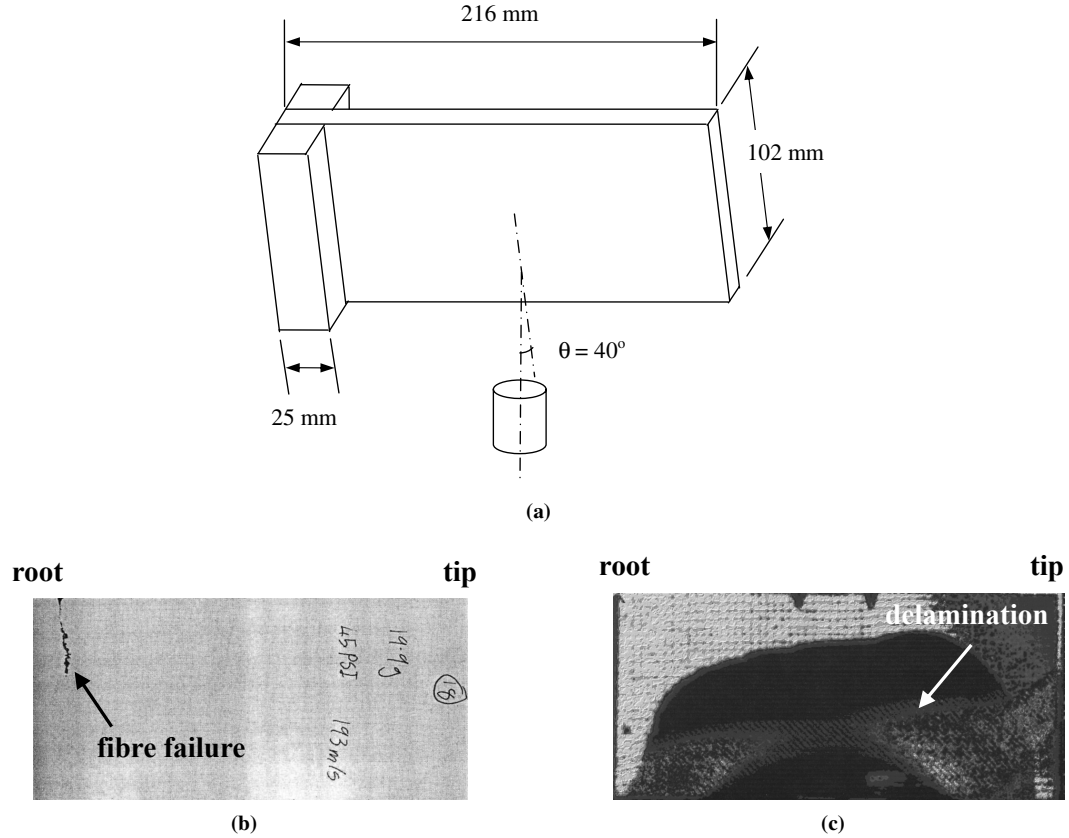

Figure 3: (a) Configuration of the cantilevered gelatine impact test outlined in [20]; (b) C-scan result from a Fibredux 914C-713-40 plate with a higher-mass ($19.9g$) lower-velocity ($193m/s$) projectile, and (c) C-scan result from an AS4/PR520 plate using a lower-mass ($10g$), higher-velocity ($306m/s$) projectile

It can be identified that although composites' delamination is well characterised at coupon scale by numerous studies in the literature, there is a gap in bridging smaller length scales to full structural component scale. It is particularly the case for high-rate, soft-body impact behaviour where component performance can not be assumed to be the same as that observed in coupon tests. The current study has therefore set out to achieve the following:

- A novel soft-body impact test which employs a large-scale specimen geometry relative to that used in the SBBB test (in-plane dimensions $200mm \times 20mm$) [18] and produces a large, scalable delamination in the laminate; the in-plane dimensions should not fall below the largest example currently observed in a delamination test ($216mm \times 102mm$ in [20]);

- A test suitable for high strain-rates, via impact loading, in order to provide representative loading conditions of a real in-flight impact, which would occur at an impact velocity of between $100m/s$ and $200m/s$;

- A test specimen suitable for through-thickness reinforcement (TTR) e.g. (Z-pins);
- A test that allows for variation in the amount of damage, and ideally failure behaviour, through modification of the impactor configuration in terms of velocity, incidence angle and impact location.

2 Test development

The general strategy used in the production of the final test design is outlined here along with justification for each of the design decisions in terms of specimen geometry and projectile impact profile.

Given the objectives outlined in Section 1, soft-body gas-gun testing was selected as the test method as it is capable of meeting these requirements. The use of a soft-body gas-gun impact test allowed for sufficient velocities – between 100-200m/s – and corresponding failure conditions to be representative of an impact during take-off or landing phases of forward flight. For simplicity, the specimen would not be subjected to any static preload (to simulate centrifugal forces) prior to impact. Based on the observations from the Soft-Body Beam Bending (SBBB) behaviour [19], a test was required which allowed for delamination propagation across a larger area, with a more varied form of delamination possible (ideally across a range of mode-ratios). Using a cantilever-type test format gives versatility afforded by only a single end being clamped. If a cantilevered design was used, then the amount of plate bending and twist generated could be varied by modifying the impact location of the projectile on the specimen surface. It was therefore proposed that one end of the current test specimen be left unconstrained – i.e. the specimen would be in a cantilevered configuration (Figure 4) in order to give the greatest versatility in bending deflections generated. A large surface area was also desired across which delamination could propagate – and thus the test would make use of a specimen of sufficient width rather than a very narrow beam (Figure 5). In order to generate sufficient bending under impact loading to give a high probability of generating delamination cracks, the aspect ratio was set above $L_x/L_y = 1.5$ - where L_x and L_y are specimen length and width dimensions respectively - such that the specimen had at least 50% more length than width. The available manufacturing in-plane bed-size was also 300mm x 250mm for implementation of Z-pins - and though this was outwith the scope of this study, it was desirable to allow for this in a further study. Based on these limitations, a final specimen in-plane geometry of 290mm x 180mm was set.

The test was aimed to balance the 0° ply compressive stresses in the root region with the delamination observed

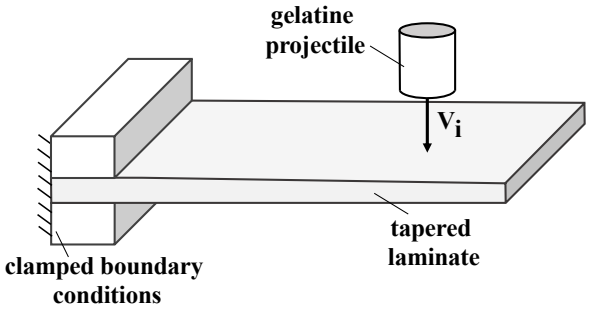

Figure 4: Basic form of the test concept: a cylindrical gelatine projectile is fired axially at a tapered, cantilevered composite laminate which is clamped between two end-plates

in the laminate. It was necessary to achieve a large amount of delamination - ideally on a single, primary delamination interface - while maintaining stress levels which did not cause substantial risk of fibre failure. There were thus two main risks associated with the test design:

Risk 1: *No delamination*, where the test failed to produce any delamination or delamination of insufficient scale to be useful;

Risk 2: *Fibre failure*, where the specimen underwent such significant bending that substantial fibre failure - possibly resulting in full section-failure of the specimen - occurred near the root.

It was necessary to develop enough bending to cause crack initiation and propagation, but with minimisation of any fibre failure near the root. It was therefore proposed to taper the laminate via lengthwise ply-drops to allow for a large thickness near the root (to provide root strength) and a smaller thickness near the tip (to encourage bending) such that both requirements were met. To maintain a simple design with reduced manufacturing costs, the taper was single-sided such that one surface was flat. A uniform-thickness region was retained near the root where the specimen was to be clamped into the root fixture. Specimen width, thickness and taper ratio were configured to generate test behaviour fulfilling the objectives described above. To achieve a high root-strength, the IM7/8552 laminate was defined by a bespoke layup which was 0°-dominated but contained features such as blocked continuous plies and orientation differences of 90° between adjacent plies to promote the required delamination. A single 4×4 plain-weave M21/IMA woven ply was included on each surface to provide impact protection to the underlying UD plies. The layup is illustrated in Figure 6.

In terms of the projectile, a gelatine impactor of cylindrical axial profile was used (Figure 4). The selected light gas-gun had a bore of $70mm$, and the gelatine mould used gave a projectile of the geometry shown in

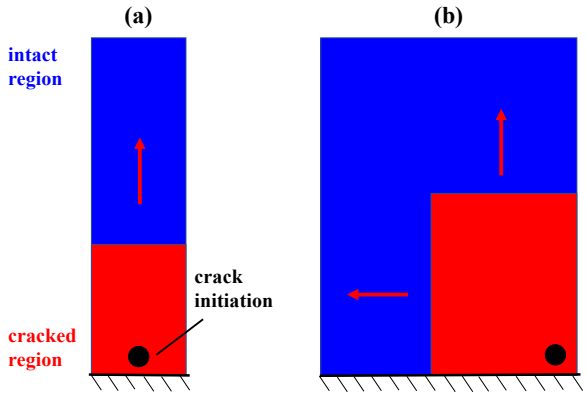

Figure 5: Illustration of the effect of increasing surface area on the potential crack propagation behaviour: (a) shows a narrow specimen, in which the crack propagates only in a single direction, but (b) shows a wider specimen where the crack may propagate in at least two directions

Figure 7. The 'rounded nose' was designed so that any slight misalignment would not have a great effect on the delamination results (as observed with the flat-fronted projectile in the SBBB tests). The lengthened body relative to diameter would give a sustained pressure pulse on the laminate surface and encourage greater bending, and the axial shot would provide a small 'projectile footprint' which would allow for greater degree of variation in the impact location depending on the test requirements. The projectile impact location (off-axis and near the laminate tip) was selected to generate a substantial amount of bending and twist, and the incident angle (15° to the surface of the laminate) was chosen to control the flow of gelatine across the surface after impact.

For boundary conditions, it was proposed that the test specimen be clamped between two plates with clamping pressure provided by torque bolts. The clamped length of laminate was set at $l_c = 30mm$, based on a clamping length of approximately 10% laminate length in prior work [20]. Fibre-failure at the plate roots was avoided by using a radius ($r_c = 15mm$) on the clamping blocks to prevent stress concentrations. Taking all of the above test design choices and limitations into account, the resultant test design is outlined in terms of geometry by Figure 8. It should be noted that the experimental results presented in this study are specific to this particular material, geometry & test parameter configuration, and alteration of parameters such as the laminate geometry, layup or projectile incident angle or velocity would also alter the test results observed. In-depth exploration of the possible outcomes of test design changes is considered outwith the scope of this study.

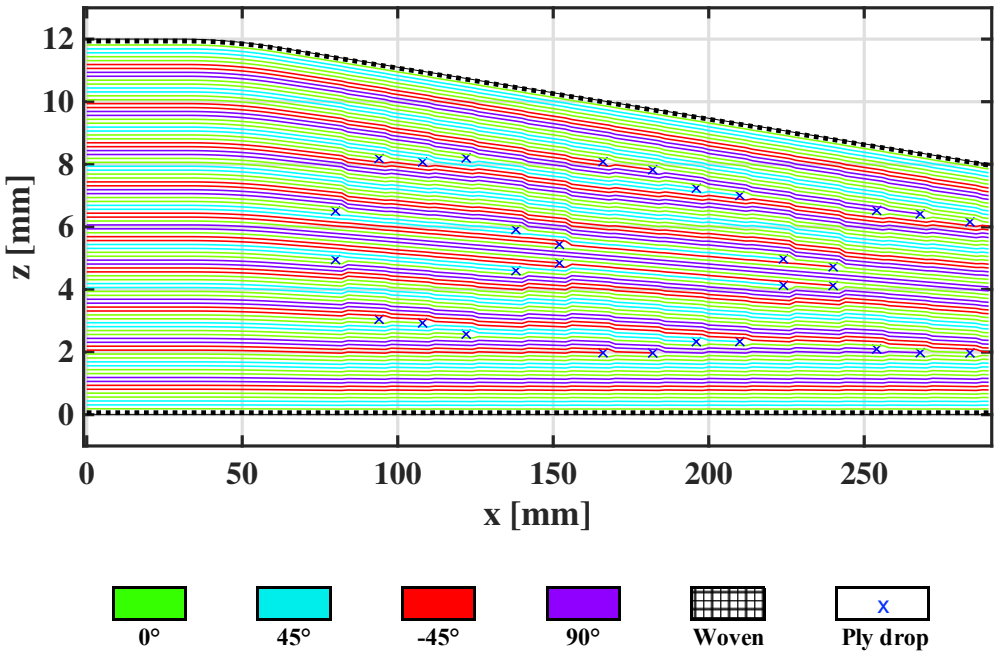

Figure 6: Illustration of the tapered laminate layup, showing the woven ply on the upper and lower surfaces and with locations of ply terminations highlighted

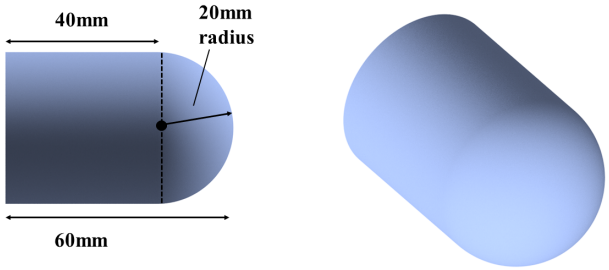

Figure 7: 'Rounded cylinder' projectile design, showing key dimensions

3 Manufacture & testing

3.1 Specimen manufacture

Six specimens were manufactured for gas-gun impact testing. The specimen was designed using a simple geometry in order to minimise manufacturing costs. It used one-dimensional, single-sided taper and was

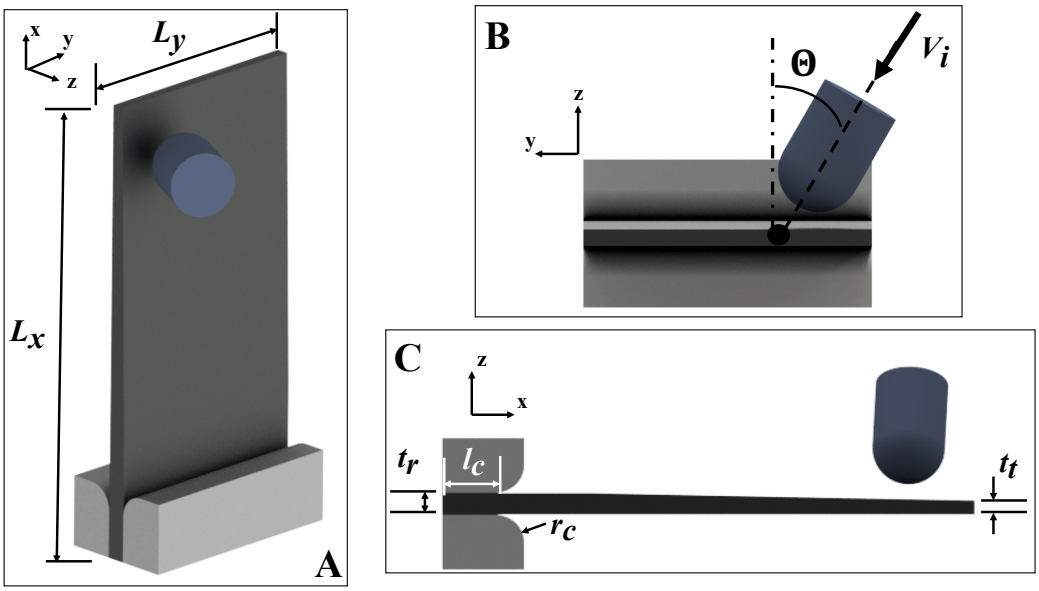

L_x [mm]	L_y [mm]	t_r/t_t	t_r [mm]	V_i [m/s]	Θ [°]	(p_x, p_y) [mm, mm]	d_i [mm]	l_i [mm]	m_i [g]	l_c [mm]	r_c [mm]
290	180	3/2	12	145	15	(270,20)	40	60	62	30	15

Figure 8: Top) Schematic representations of the final test configuration: A) Isometric; B) viewed along $x-$axis and C) viewed along $y-$axis schematic representations of the final test configuration; Bottom) the numeric values for key parameters associated with the final design, where (px, py) are the $x-$ and $y-$ co-ordinates of impact relative to the specimen edges at $x = 0mm$ and $y = 0mm$ on the impact side; d_i is the diameter of the nose of the impactor; l_i is the total length of the impactor; m_i is the nominal mass of the impactor; l_c is the clamped length of the laminate in the $x-$ direction, and r_c is the radius of the fillet on the fixture edge contacting the laminate

manufactured using hand-layup using from unidirectional (UD) IM7/8552 pre-preg material with an M21/IMA wovenpre-preg surface protective layer. In order to facilitate simple manufacturing, soft top tooling was employed such that complex tooling parts did not require machining at considerable expense. A silicone sheet was placed on top of the laminate above the release film and beneath the vacuum bag, and also beneath the laminate between the release film and the tool plate. The use of silicone sheet was in order to maintain consistency with the manufacture of Z-pinned laminates which would be the subject of a further study.

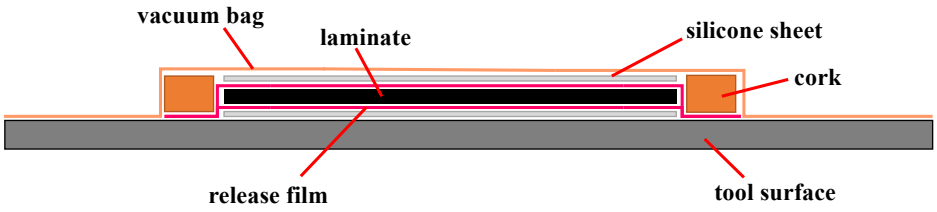

Figure 9: Schematic diagram of the vacuum-bagging configuration for each laminate, showing use of $3mm$ silicone sheeting between the upper laminate surface and the vacuum bag, and lower laminate surfaces and tool-plate

Specimens were cured using a standard IM7/8552 aerospace autoclave curing cycle [22]. The laminates were

then de-bagged and trimmed to the designed in-plane dimensions using a water-jet cutting facility. Specimen thicknesses were measured at several points; specific data regarding specimen thickness is presented in Section 3.3.

3.2 Experimental setup & test method

The design process resulted in a test configuration which produced a bending response in a tapered, cantilevered composite plate that was sufficient to initiate delamination near the root without inducing fibre failure. The test was sized and tailored to produce the desired result within physical constraints of available equipment and manufacturing facilities. The manufactured specimens were subjected to high-speed gelatine gas-gun impact testing to generate results for the study of large-scale delamination propagation at high rate.

The test made use of a light gas-gun facility (Figure 10)) which was used to accelerate a gelatine projectile within a foam sabot to impact velocity. The gas-gun had a gun bore of $70mm$. The gelatine was made via an aqueous solution of powdered ballistic gelatine and water (Figure 11(a)). The sabot was manufactured from polyurethane foam inside a closed mould and sanded to remove unfavourable surface roughness or imperfections, subsequently greased by hand and rammed to its firing position at the base of the barrel (Figure 11(b)).

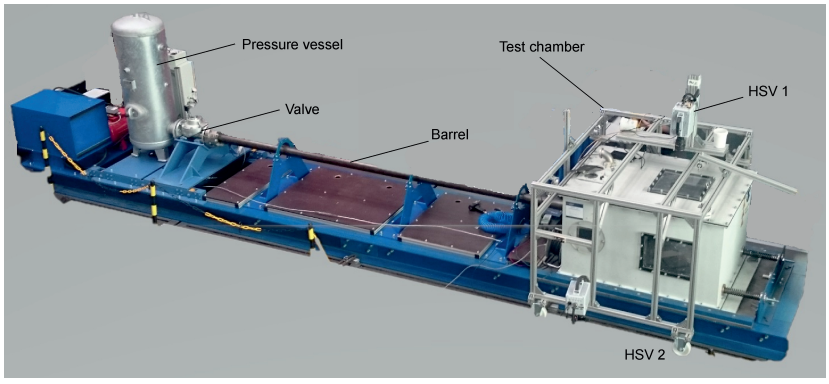

Figure 10: Photograph of gas-gun configuration with key components indicated

The specimen clamping assembly was designed and built by TU Dresden and the technical design is shown in Figure 12. Eight $M10$ bolts connected the two clamping plates and were used to apply clamping pressure to the specimen surfaces. The entire test fixture was located within an impact-resistant metallic chamber which contained transparent plastic windows to allow for viewing and high-speed camera recording of the impact event. The as-manufactured tapered composite beams were mechanically clamped into the fixture at the flat, thick root end and the clamping bolts were initially hand-tightened followed by application of a precise torque of $30Nm$

(a) **(b)** **(c)**

Figure 11: (a) Rounded-end gelatine shot post-trimming and pre-marking for firing; (b) Foam sabot post-sanding and pre-greasing for firing; (c) Gelatine with nose painted placed into sabot before being placed into firing position

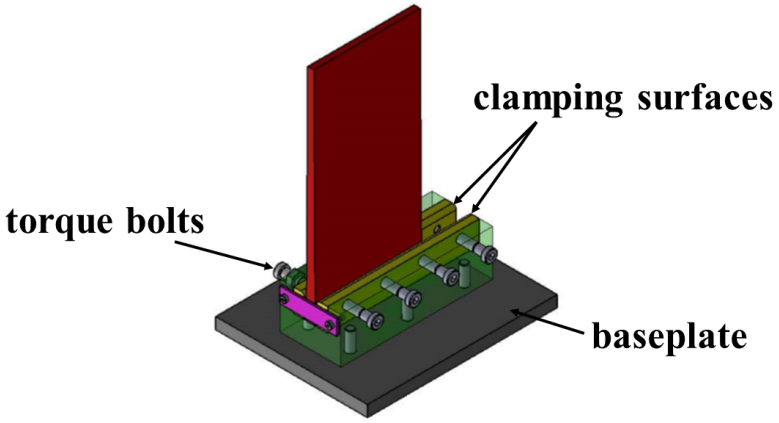

Figure 12: CAD drawing of the test fixture assembly, showing the arrangement of the *baseplate* and *clamping mechanism* with respect to the *laminate position*.

using a torque-wrench. The enclosure had a removable lid which was bolted in place using a pneumatic drill. The pressure vessel was pressurised to a prescribed value based on prior calibration in order to generate the correct projectile velocity on firing. Trial shots were conducted against a dummy steel plate to verify the gelatine velocity and shape. The test environment was not temperature-controlled or under vacuum, and the tests took place in ambient environmental conditions - though temperature was monitored to ensure the tests took place at approximately normal room temperature ($25°C$)

Quantitative measurements of projectile velocity and specimen deflections were taken through two Photron FASTCAM SA4 high-speed cameras running at $25,000$fps. The cameras were positioned orthogonal to the short tip-face of the laminate (*HSV1*) and orthogonal to the long edge furthest from impact (*HSV2*) as illustrated in Figure 13. Figures 13(c) and 13(d) show approximately the view seen through each high-speed camera.

Scale-bars are visible orthogonal to the view for *HSV1* (Figure 13(c)) allowing for accurate calculation of both impact velocity and tip deflections in postprocessing via known scale lengths. Prior to impact, specimens were coated in matt white paint and marked with a series of lines and dots (configuration shown in Figure 14) to allow for easier measurement of deflections and crack propagation. Use of white paint allowed cracks to be visualised along edges. Dots were used to aid in tracking of the two sub-laminates after delamination near the mid-plane. The coating used was a solvent-based alkyd paint.

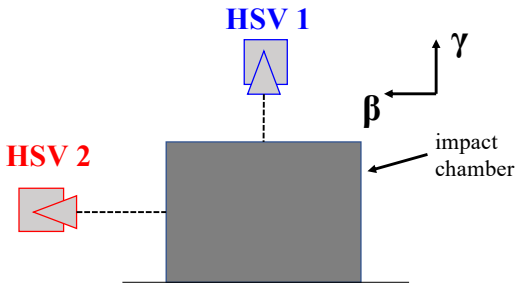

(a) Schematic diagram of high-speed video camera (HSV) configuration viewed along gas-gun $\alpha-$axis, showing *HSV1* above impact chamber pointing vertically downwards (in $\beta-$direction) and *HSV2* pointed orthogonally at the long edge of the specimen

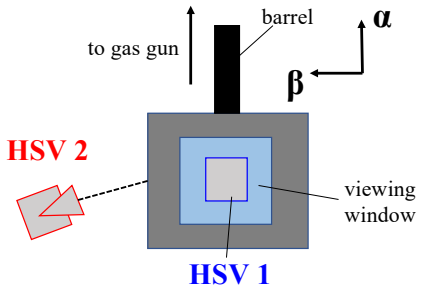

(b) rotated version of diagram (a) viewed along the gas-gun γ-axis

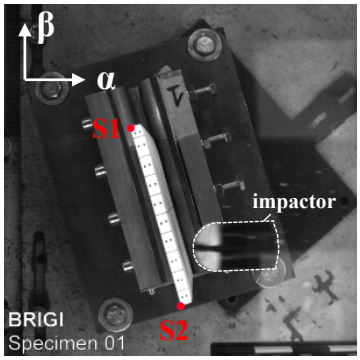

(c) Still from *HSV1* showing displacement measurement points *S1* and *S2*

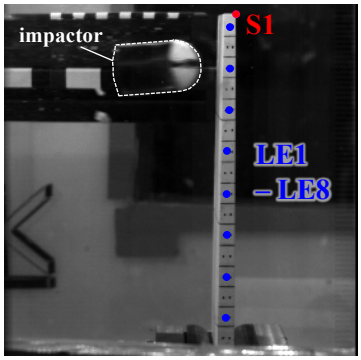

(d) Still from *HSV2* showing displacement measurement points *S1* and *LE1-LE8*

Figure 13

Six specimens were tested using the test design parameters. The design process intended to reduce or prevent the need for the many trial tests which could precede full testing at the 'optimal' set of parameters by eliminating the need to tune experimental parameters. Experimental trials are costly and introduce the risk of being unable to obtain the optimal set of parameters in the set amount of time or number of specimens available. During the design phase, an initial test velocity of $V_i = 145m/s$ was selected to attempt to generate an initial delamination near the root and close to the laminate mid-plane by global bending and propagate the delamination through structural deflections. Delamination extent in all cases was measured using ultrasonic C-scanning. Specimens were C-scanned using an air-coupled ultrasonic scanning system before and after each test. Crack propagation

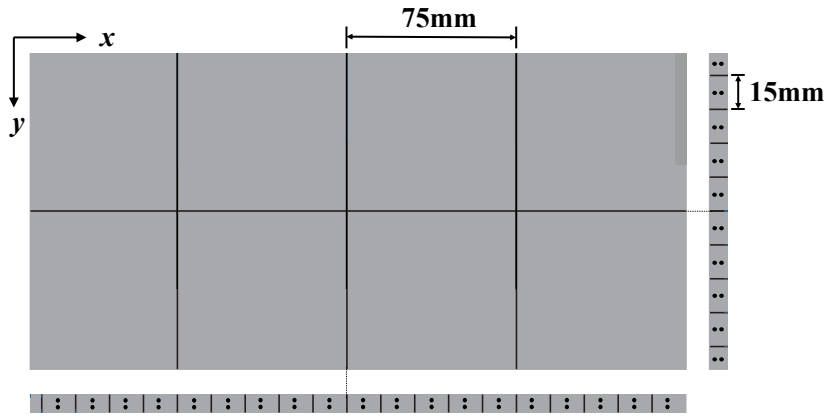

Figure 14: Sketch of the mark-up configuration on the laminate surface, showing location of lines and dots. Two end-projections are shown on the *bottom* and *right* of the base diagram, which shows the laminate upper surface. Taper has been omitted for clarity

was also observed via tracking the crack tip along the long edge using *HSV2*. Specimen deflections and gelatine behaviour were observed using both *HSVs*.

3.3 Results

Table 1 summarises the test results. The average measured root and tip thicknesses are given, with an average root thickness of $t_r = 12.7mm$ (6.2% over nominal) and tip thickness of $t_t = 9.0mm$ (13.1% over nominal). The average gelatine mass is $71.4g$, which is approximately 20% over the nominal gelatine mass due to the experimental gelatine used. The initial test velocity based on finite element analysis was set at $V_i = 145m/s$. This was intended to initiate delamination near the root and also propagate it sufficiently such that, were through-thickness reinforcement present, the delamination would be sufficient to examine the effect of the reinforcement. For the test *CP1*, the result was satisfactory; however, the repeat test *CP2* did not produce sufficient delamination, and so test velocity was increased across tests *CP3* and *CP4* until substantial delamination was achieved again. A large amount of delamination occurred in test *CP4*, at a new test velocity of $V_i = 164.8m/s$. Due to this producing a satisfactory delamination result, the test velocity set-point thereafter was set at $V_i = 165m/s$. An average delaminated area A_d of 80% ($CoV = 0.231$) was measured for all tests at a nominal velocity of $V_i = 165m/s$. Firing velocity was achieved across all tests to within $\pm 2.5ms$ of nominal.

Table 1: Results for the unpinned gelatine impact tests

Specimen ID	Tip thickness [mm]	Root thickness [mm]	Gelatine mass [g]	Velocity [m/s]	Impact Energy [J]	A_d [%]
CP1	9.0	12.8	70.4	145.0	740.2	47
CP1	9.1	12.8	71.8	145.0	754.9	24
CP3	9.1	12.9	73.3	154.0	880.4	25
CP4	9.0	12.7	70.0	164.8	950.4	64
CP5	9.0	12.7	71.9	166.1	992.1	75
CP6	9.1	12.8	71.3	165.2	972.2	100

3.4 Experimental observations

3.4.1 Impact response

HSV footage was examined to determine the dynamic response of the specimen, in terms of general behaviour after impact, measured deflections and crack propagation. Figure 15 shows a typical deflection profile observed from *HSV1* and *HSV2*, and Figure 16 shows a more detailed sequence of images illustrating longitudinal bending and crack progression from *HSV2*. It is clear that the specimen undergoes substantial longitudinal and twisting deflections, and that delamination initiation and propagation is driven by global bending deflections of the laminate.

While it is difficult to ascertain exactly where delamination initiates, it is likely that the initiation point is in the root region farthest from the impact location where intuitively there is the greatest amount of interlaminar shearing due to high levels of both bending and twisting. Delamination initiation will likely either occur during the initial downward twisting deflection (Figure 15(b) and Figure 15(e)) immediately after impact or on the reversed twisting deflection (Figure 15(c) and Figure 15(f)).

After initiation, the majority of crack propagation appears to occur rapidly during the reversed transverse deflection (Figure 15(c) and Figure 15(f) and between Figure 16(a) and Figure 16(b)). Crack propagation rate is estimated from the *HSV2* footage to be in the order of $V_c = 150m/s$. The plate appears to remain deflected away

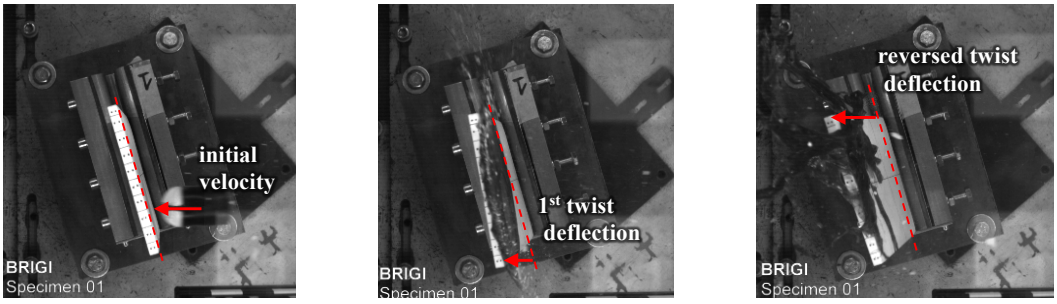

(a) time = $0ms$ **(b)** time = $1ms$ **(c)** time = $3ms$

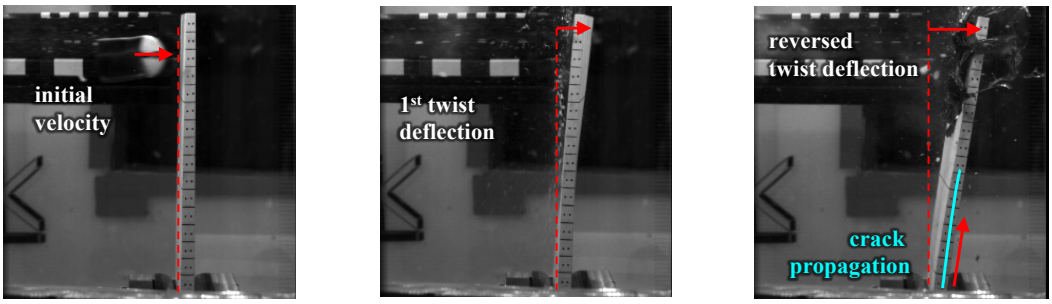

(d) time = $0ms$ **(e)** time = $1ms$ **(f)** time = $3ms$

Figure 15: Typical dynamic response (case *CP1* with $V_i = 145m/s$) viewed from both *HSV1* (top) and *HSV2* (bottom), showing transverse deflection and corresponding crack propagation behaviour

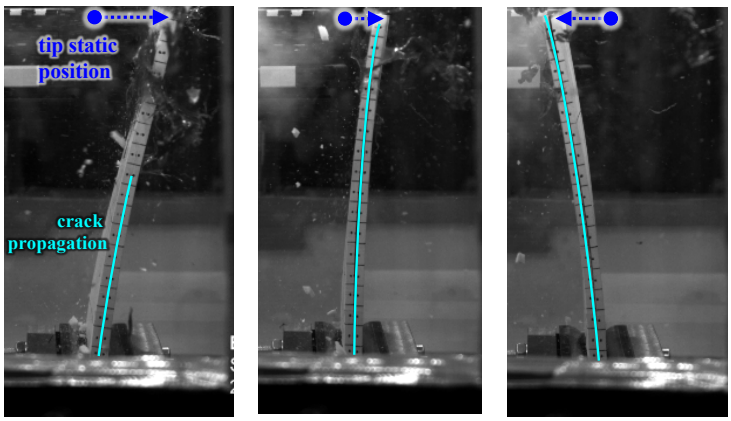

(a) time = $3ms$ **(b)** time = $5ms$ **(c)** time = $8ms$

Figure 16: Typical deflection time sequence during crack propagation showing movement of the (nearest) tip in the *HSV2* footage for case *CP6* with $V_i = 165m/s$

from the impact for some time while the crack propagates. The 'sustained pulse' of bending coincides with crack propagation, suggesting that the plate is losing stiffness during cracking. The gelatine clearly flows from one side of the specimen, across the width and then continues across the surface of the specimen in a chordwise manner until it departs the specimen surface (Figure 15). An interesting observation is that while the gelatine appears to flow in a fluid-like manner in the high-speed video footage (e.g. in Figure 15), the retrieved fired gelatine obtains

much of its pre-impact mass and largely remains as a single continuous structure (Figure 17).

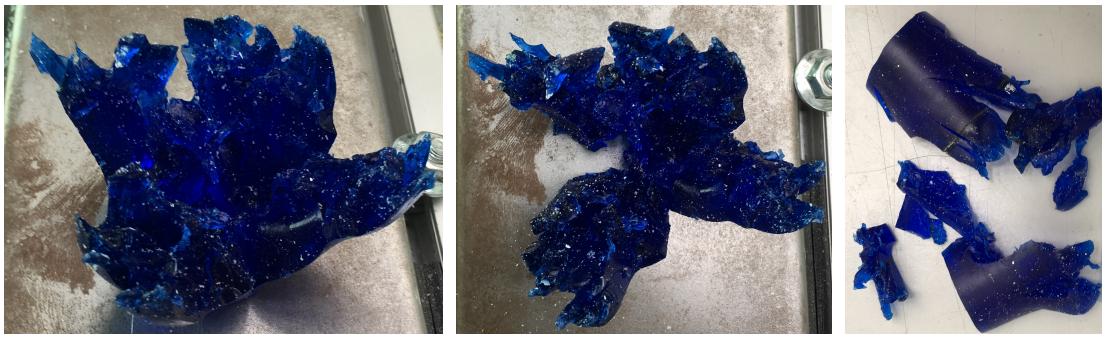

(a) *CP1* **(b)** *CP1* (2nd view) **(c)** *CP2*

Figure 17: Retrieved gelatine from cases *CP1* (Figure 17(a) and 17(b)) and *CP2* (Figure 17(c)), both using a test velocity of $V_i = 145m/s$, showing gelatine damage and intact nature of projectiles post-impact

3.4.2 Deflection measurements

The plate tip deflection response over time was measured using high-speed video (HSV) tracking. Figures 13(c) and 13(d) show the different measurement locations annotated on the *HSV* camera views. Tip deflection and twist were generated by measurement of the locations *S1* and *S2* from *HSV1*, while the beam bending behaviour was obtained from locations *LE1* - *LE8* in the *HSV2* footage. Measurements were taken at $0.5ms$ sample intervals from the HSV footage for each of these displacement tracking locations. Translational displacements were measured along the global gas-gun $\alpha-$axis. Plots of tip deflection from locations *S1* and *S2* are given in Figure 18(a) and 18(b).

The overall beam deflection response at maximum negative deflection ($-$ve $\alpha-$axis direction) and subsequent maximum reversed deflection (+ve $\alpha-$axis direction) from the points *LE1* - *LE8* along the span in *HSV2* is given in terms of the averaged result measured for each V_i in Figure 19(a), and for each distinct test undertaken at the final test velocity of $V_i = 165m/s$ in Figure 19(b). Figure 20 shows the twist calculated from the $\alpha-$axis displacements of points *S1* and *S2* where this is considered positive for anti-clockwise motion around the specimen local $x-$axis when viewed from tip to root. Figure 20(a) shows the average twist calculated from results at each test velocity, while Figure 20(b) shows each individual result for the cases at $V_i = 165m/s$. In order to better contextualise the tip deflection and twist plots, images of cases at each test speed used are presented at their static position and at their maximum initial and reversed deflections - from the perspective of both *HSV1* and *HSV2* - in Figures 22 and 21 respectively.

There appears to be little change in behaviour between tests *CP2* and *CP3*, which show a very similar displacement response and yet were conducted at two different speeds of $V_i = 145m/s$ and $155m/s$ respectively. Conversely, tests *CP1* and *CP2* were both carried out at $V_i = 145m/s$ and yet exhibit greater differences in their deflection responses. There are also no significant differences in the projectile masses or laminate thicknesses measured before each test and given in Table 1. It is possible that there is a very high sensitivity of the test results to even minor changes in the test parameters such as projectile mass & velocity, and it is notable that for tests using ballistic gelatine, the projectile properties may vary with the environmental conditions and this could lead to differences in the results. However, it is likely that the delamination condition of each laminate during the test has a large influence on the deflection results, and should be considered further. This effect is discussed in detail in the following section.

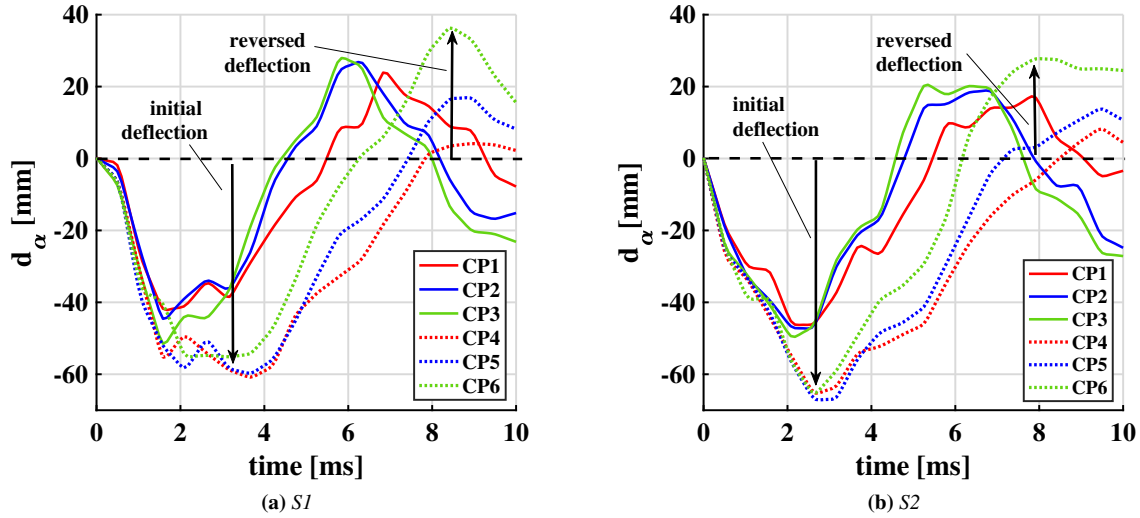

(a) *S1* **(b)** *S2*

Figure 18: $\alpha-$axis tip displacements from tests CP1 - CP6 on unpinned laminates showing data taken from point *S1* (a) and points *S2* (b) with points of initial and reversed full deflections highlighted

3.4.3 Delamination

Figure 23 shows the ultrasonic C-scan results for delamination for all specimens. Analysis of the ultrasonic C-scans of the pristine laminates taken before each test showed no evidence of any delamination or other damage. It is evident that tests *CP2* and *CP3* have the least delamination area, while the specimens *CP1* and *CP4-6* are significantly more delaminated. As previously highlighted, the differences in deflection behaviour shown across Figures 18 - 22 are likely to be related to the differences in the amount of delamination occurring in each specimen. For the more intact specimens, the response is characterised by shallower deflections and initial

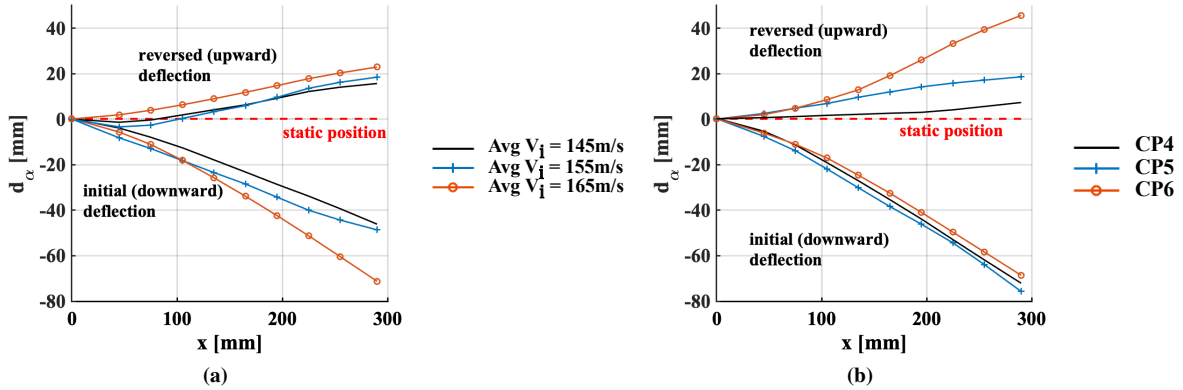

Figure 19: Variation in the $\alpha-$axis displacement of each point *LE1 - LE8* showing a side-on profile view of the minimum and maximum displacements across all points in time; (a) shows average results observed at each distinct test speed and (b) shows results for each test (CP4 - CP6) at the ultimate test velocity $V_i = 165m/s$

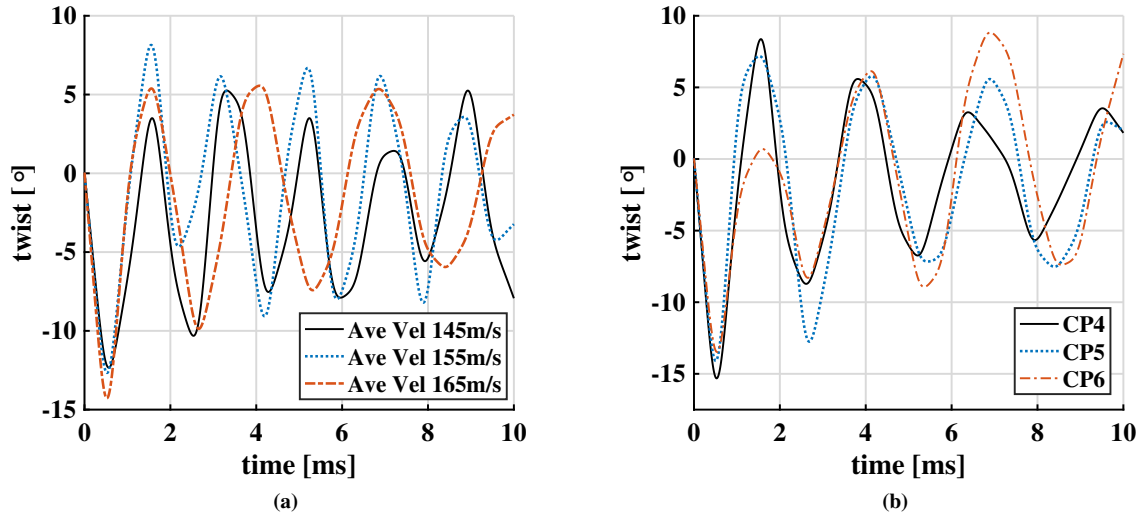

Figure 20: Specimen twist extracted from the difference in tip displacements from points *S2* and *S1*, with twist being taken as +ve anti-clockwise when viewed along the specimen $x-$axis from tip to root. (a) shows the twist values averaged across all tests at each test velocity V_i (145, 155 and $165m/s$) and (b) shows the twist values for each individual test at $V_i = 165m/s$ (CP4, CP5 and CP6)

bending deflections that are quickly reversed. Twist in cases where specimens remain more intact tends to reduce over time. For tests which show greater delamination, there is a tendency for the displacement result to enlarge over time – as indicated in the analysis of HSV footage – and this appears to happen after the onset of crack initiation and initial propagation. Twist in cases with substantial levels of delamination seems to either remain large or increase over time. The time-displacement relationships suggests that once the specimen reaches a certain tip displacement, delamination initiates and quickly propagates, causing a loss of stiffness which then causes subsequent further displacement, etc. There is also an increase in the period of the deflection cycle for

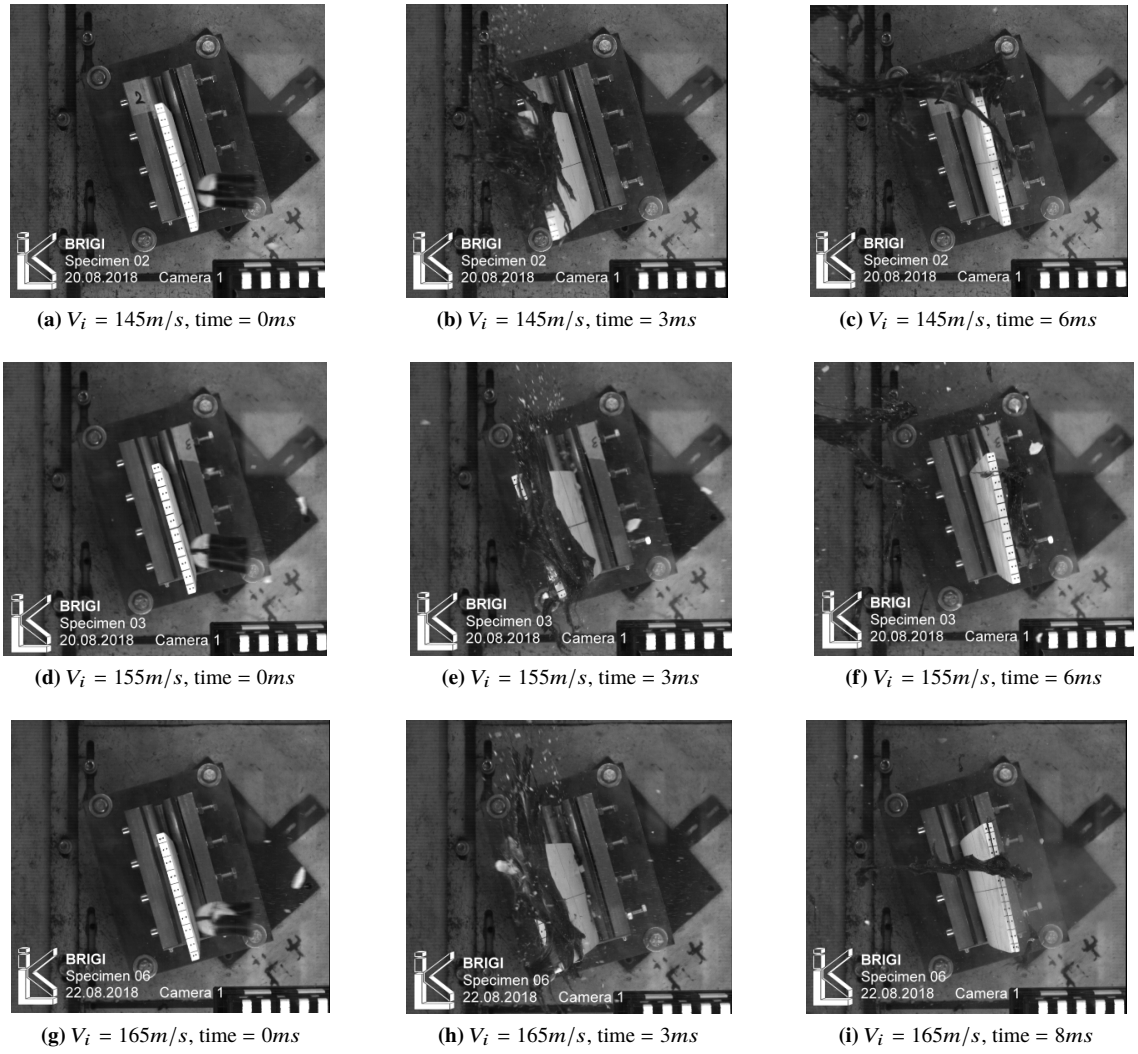

(a) $V_i = 145m/s$, time = $0ms$ **(b)** $V_i = 145m/s$, time = $3ms$ **(c)** $V_i = 145m/s$, time = $6ms$

(d) $V_i = 155m/s$, time = $0ms$ **(e)** $V_i = 155m/s$, time = $3ms$ **(f)** $V_i = 155m/s$, time = $6ms$

(g) $V_i = 165m/s$, time = $0ms$ **(h)** $V_i = 165m/s$, time = $3ms$ **(i)** $V_i = 165m/s$, time = $8ms$

Figure 21: Dynamic response behaviour for three cases *CP2*, *CP3* and *CP6* at $V_i = 145m/s, 155m/s$ and $165m/s$ viewed from *HSV1*

more delaminated specimens. Overall, this behaviour suggests a strong link between delamination within each specimen and the observed deflections.

Considering the data shown in Table 1 and the delamination profiles of the plate area shown in Figure 23, it is clear that the delamination area A_d is scalable depending on the test velocity used. Figure 25 shows the *normalised delamination area* - the amount of delaminated surface area A_d measured from the 2-D C-scan profile relative to the overall specimen in-plane area - calculated using A_d = (delaminated area/total specimen area) for each of the tests. Test *CP1* shows a much larger amount of delamination than tests *CP2* or *CP3*, with a clear outline of the projectile imprint indicating local delamination has occurred near the impact zone. However, tests *CP2* and *CP3* – conducted at different speeds – show virtually no difference in the delamination result.

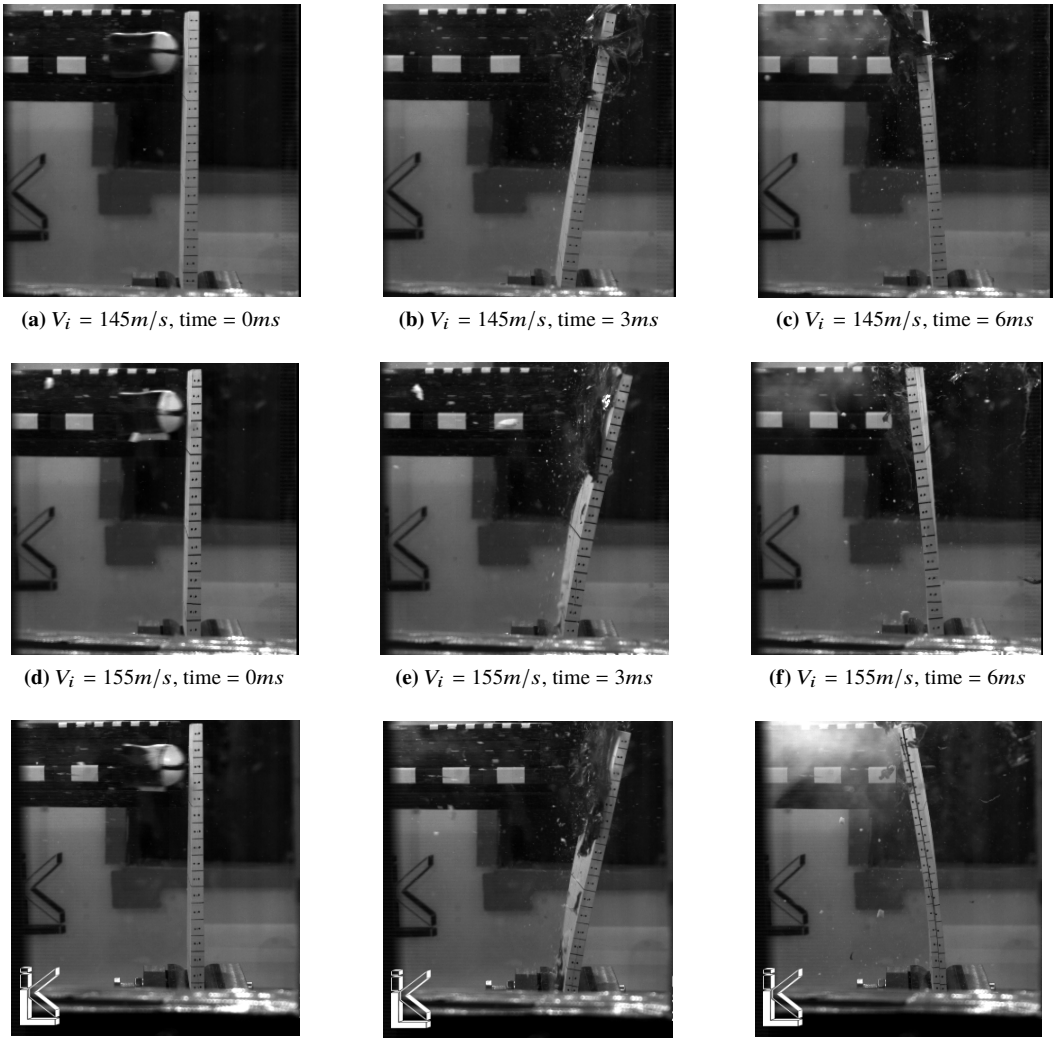

(a) $V_i = 145m/s$, time = $0ms$ **(b)** $V_i = 145m/s$, time = $3ms$ **(c)** $V_i = 145m/s$, time = $6ms$

(d) $V_i = 155m/s$, time = $0ms$ **(e)** $V_i = 155m/s$, time = $3ms$ **(f)** $V_i = 155m/s$, time = $6ms$

(g) $V_i = 165m/s$, time = $0ms$ **(h)** $V_i = 165m/s$, time = $3ms$ **(i)** $V_i = 165m/s$, time = $8ms$

Figure 22: Dynamic response behaviour for three cases *CP2*, *CP3* and *CP6* at $V_i = 145m/s, 155m/s$ and $165m/s$ viewed from *HSV2*

Considering the laminate thicknesses, gelatine mass and velocity as detailed in Table 1 for the tests, there appears to be no significant discrepancies. It is therefore assumed that *CP1* is an outlier and it is not taken as standard behaviour for a test shot at $V_i = 145m/s$.

Tests *CP4-6* use a test velocity of $V_i = 165m/s$. From the measured velocities in Table 1 the gas-gun reproduces this velocity to within $\pm 2m/s$. However, from the delamination C-scans in Fig. 23, the test result is clearly highly sensitive to even slight changes in the test environment and parameters or specimen to specimen variation.

Examination of the specimens after testing shows that there is one predominant delamination interface close to

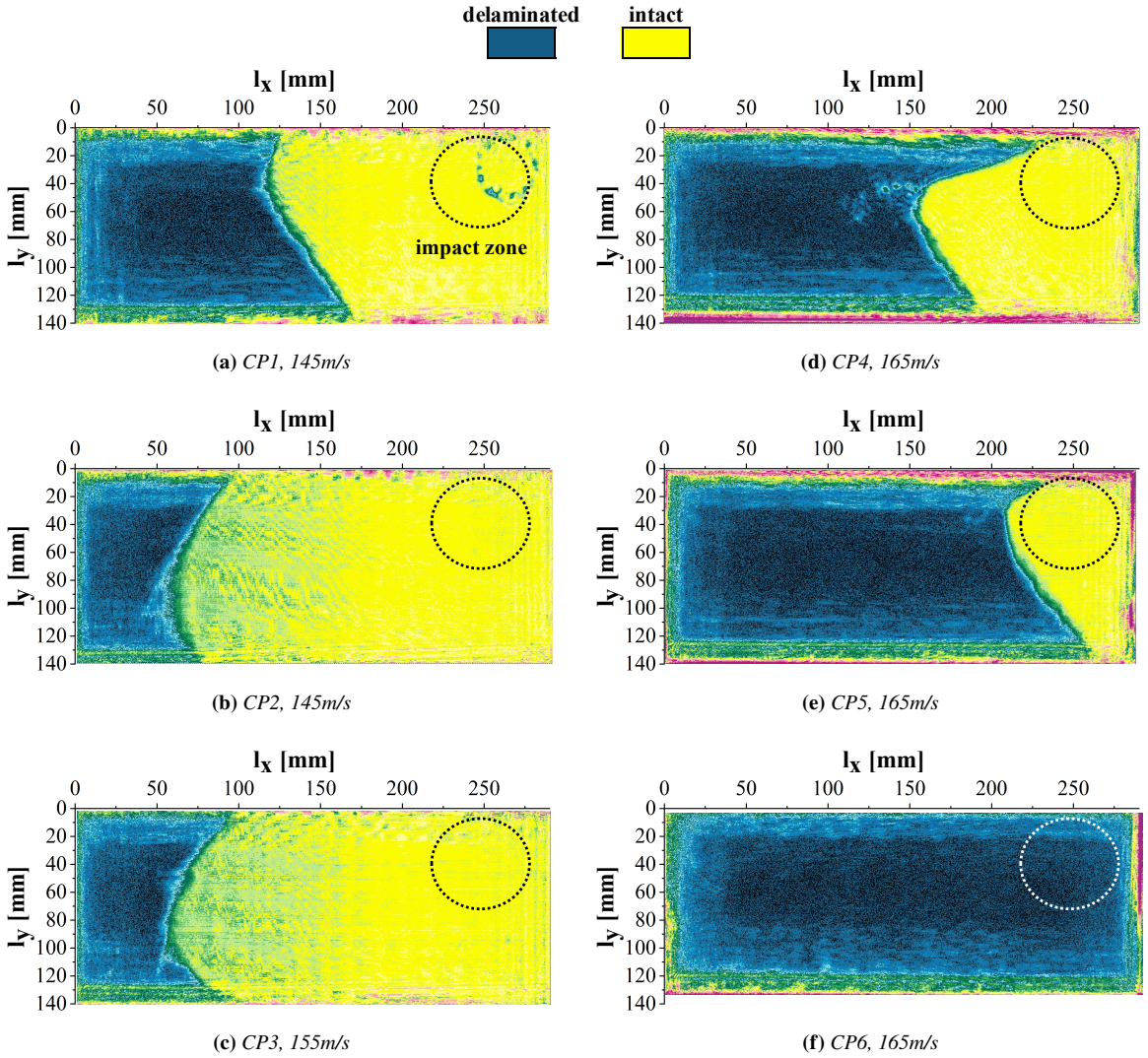

(a) *CP1, 145m/s*

(d) *CP4, 165m/s*

(b) *CP2, 145m/s*

(e) *CP5, 165m/s*

(c) *CP3, 155m/s*

(f) *CP6, 165m/s*

Figure 23: C-scan plots of delamination for unpinned laminates *CP1 - CP6*, showing region of impact. The specimen root corresponds to $l_x = 0mm$, the visible edge in *HSV1* corresponds to $l_x = 290mm$ and the visible edge in HSV2 corresponds to $l_y = 140mm$.

the mid-plane of the laminate and this is shown for test *CP5* in Figure 24. Delamination primarily occurs at the same or very similar through thickness location during each test, which is just below the mid-plane. A number of secondary cracks are visible in certain tests which are generally confined to, or just ahead of, the region where the fixture and the laminate are in contact. Subsequent sectioning of the laminates has shown that these cracks do not extend far into the laminate away from the edge. The secondary delaminations may be considered a result of the high levels of bending in the root region and should not affect the efficacy of the test. In fact, secondary delaminations in this region could act as stress relief on the highly-stressed root region during the critical initial bending deflection.

Figure 24: Photograph taken post-impact showing evidence of a large, primary crack close to the mid-plane from test CP5; a small, secondary delamination has also been highlighted

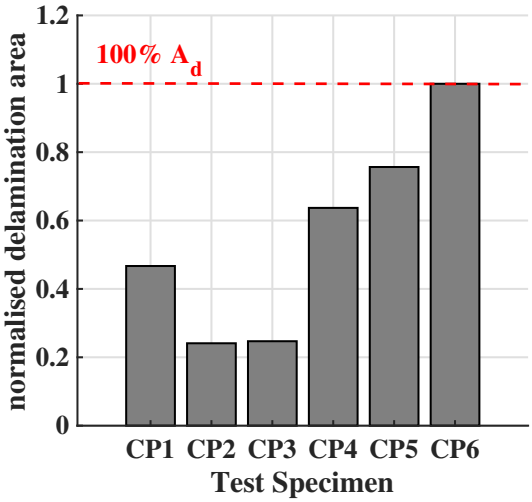

Figure 25: Normalised delamination area A_d as a fraction of the total specimen in-plane area (A_d = delaminated area/total specimen area)

The substantial variation in delaminated area across the tests performed at $V_i = 165m/s$ from a minimum of $A_d = 64\%$ to a maximum of $A_d = 100\%$ could be attributed to various factors. As mentioned previously, no C-scan results taken prior to testing showed any sign of major damage to any of the laminates, for example, delamination due to water-jet cutting or acquired during transit. It can therefore be ruled out that existing delamination in some laminates caused a difference in the delamination results due to impact. The environment in the test chamber was not temperature-controlled or under vacuum, and so it is possible that minor fluctuations in environmental conditions may have generated some differences in the responses, but conditions other than environmental temperature were not measured. Gelatine behaviour has been shown to be relatively consistent so long as temperature is maintained below a certain level, and this level was monitored and not exceeded during testing. The numerous ply-drops contained in each specimen may have contributed to the discrepancies in the results, with local variations in transverse normal stresses at the different ply drops providing many different drivers for delamination initiation and propagation. In any case, it is clear that for the given case a velocity threshold for obtaining full delamination exists - that is, there is virtually no difference in impact velocity between

obtaining $A_d = 64\%$ and $A_d = 100\%$, suggesting that the test velocity used of $V_i = 165m/s$ sits almost exactly on the velocity threshold for this specific test configuration. It is notable and acknowledged by the authors that confirmation of the test repeatability would be provided by performing more tests and obtaining more data, and it is intended that this work be continued to further understanding of the observed phenomena.

As the delamination is confined generally to a single primary interface, and variation in the delamination result is from partial (64% A_d) to full (100% A_d) delamination, this behaviour is seen as fulfilling of the requirements as set out in Section 1 for a test velocity set at $V_i = 165m/s$.

3.4.4 Gelatine behaviour

The behaviour of the gelatine during the test is complex. Detailed analysis of this behaviour is considered outside the scope of this study, however it is useful to examine the gelatine deformation as this will affect the laminate response during the test. The *CP1* case is used as a reference case based on a moderate level of delamination ($A_d = 47\%$). Figure 26 shows a comparison of the gelatine motion during the test for the *CP1* experiment from *HSV1*.

(a) $t = 0.0ms$ **(b)** $t = 0.8ms$ **(c)** $t = 3.2ms$

Figure 26: Experimental gelatine deformation; (a) - (c) show the experimental gelatine behaviour throughout the laminate deflection cycle for the *CP1* test. Gelatine motion is indicated using *white arrows*

Initial gelatine behaviour ($t \leq 0.8ms$) in the experiment (Figure 26(a) - 26(c)) shows a rapid deformation to a become a very flat mass, spreading across a large amount of the laminate upper surface. During this time period, it appears that the gelatine remains a single mass and does not fragment into different parts (shown previously in Figure 17). It moves transversely across the surface of the laminate (from tip *S2* to *S1*) before then departing the

surface. The gelatine remains on the surface until the full reversed bending deflection of the laminate (not shown in the images). Any fragmentation of the gelatine projectile only seems to occur once it departs the surface. There appears to be a significant amount of friction between the gelatine and the laminate, and the gelatine begins to depart the laminate surface while the laminate is still in downward bending. Further investigation is needed to determine the mechanisms behind the gelatine behaviour, but this data is useful in informing modelling of ballistic gelatine using e.g. using a smooth-particle hydrodynamic (SPH) material model.

4 Post-test fracture analysis

After testing, the specimen from test *CP5* was sectioned into fracture regions using a diamond saw. Thirteen fracture regions defined across the entire crack surface area, each with an upper and lower fracture surface, were selected, with the location of the fracture regions visualised on the fracture surface in Figure 27. The fracture regions were given an alphanumeric ID corresponding to the location of the fracture region. The configuration of the upper and lower fracture surfaces is that the *upper* surface corresponds to the impact side, and the *lower* surface corresponds to the opposing side to impact.

4.1 Fractographic features

The primary features which assist in determining the nature of the fracture are found on the upper fracture surface of specimen *CP5*. The features are in the form of *shear cusps*, which protrude outwards from the surface and are caused by microcracking in the matrix material as the crack propagates [23]. Figure 28(a) shows examples of shear cusps from different regions on the upper fracture surface of *CP5*.

Shear cusps may be used to infer certain crack propagation characteristics such as crack mode-ratio at failure. The out-of-plane *cusp tilt* (Figure 28) helps to identify mode-ratio, with more vertical cusps representing a more Mode II crack and flatter cusps representing a more mixed-mode crack.

Figures 28(a), 28(b) and 28(c) show samples of shear cusps taken from regions A5, A11 and A13 respectively. Considering the basis for determining mode-ratio outlined above, it can be inferred based on the cusp tilt that

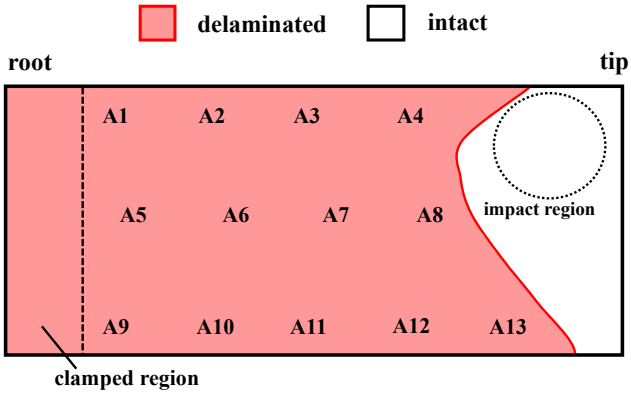

(a) Unpinned (*U/P*) sectioned specimen *CP5* (A)

Figure 27: Fracture diagram showing the delaminated region overlaid on the specimen geometry with regions e.g. *A1* selected for fracture analysis indicated

379 the mode-ratio is closer to Mode II in regions nearer the root of the plate, and more mixed-mode as the crack
380 propagates towards the tip.

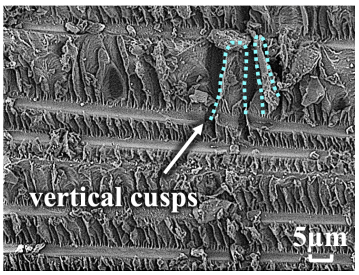

(a) SEM micrograph from region *A5* in the specimen *root region* (1800×)

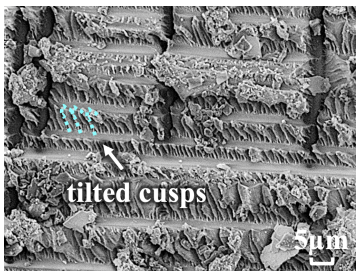

(b) SEM micrograph from region *A11* in the specimen *mid-span region* (1800×)

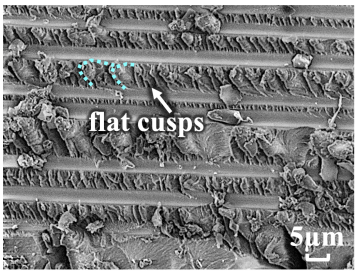

(c) SEM micrograph from region *A13* in the specimen *tip region* (1800×)

Figure 28: Illustration of the variation in cusp out-of-plane tilt with mode-ratio with corresponding SEM micrographs taken from the upper surface in Figure 27 - a) Near root, b) mid-length and c) near tip

381 This general approach was taken during post-test analysis of fracture surfaces in all regions, where qualitative
382 assessments were made regarding the cusp tilt and the possible mode-ratio was estimated. Fracture analysis
383 was performed assuming an entirely vertical cusp represented pure Mode II behaviour, and using this as a
384 reference point. This analysis was used to generate a rough 'failure map' of specimen *CP5*, and this is shown in
385 Figure 29. It is evident that while this was a qualitative analysis, there is some change in the mode-ratio as the
386 crack progresses from the root towards the tip of the specimen, and this change is a likely reduction in mode-ratio
387 towards more mixed-mode behaviour. The perceived change in mode-ratio is an interesting result and could
388 be attributed to many different mechanisms. Based on the crack progression behaviour shown in Figure 16, it
389 is possible that as the plate undergoes reversed bending, some crack opening is observed after propagating in
390 Mode II during the initial bending. Other mechanisms could be energy loss due to abrasion as fracture surfaces

rub during cracking or higher-order microcracking behaviour. Further work is necessary to determine the exact reasons for this behaviour.

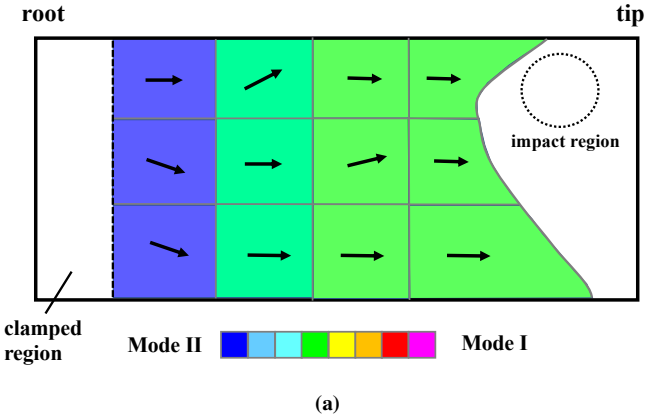

Figure 29: Qualitative mode-mixity and crack direction failure map of specimen *CP5*, where the mode-ratio and crack-growth direction are presented. A colour-map is used to represent the severity of the mode-ratio change based on observed features for visualisation purposes *only*

5 Conclusions

A novel test method has been presented for large-scale, high strain-rate delamination failure performance of sub-element scale composite structures. The test method made use of a light gas-gun and cylindrical gelatine projectile which was used to impact a tapered, cantilevered, pre-preg composite plate at incidence and with high velocity in an off-centre location to invoke large reversed bending deflections. The test method was developed in the context of a requirement to create large-scale delamination. In future work it can be used to benchmark through-thickness reinforcement technologies, such as Z-pins, when encountering delamination failure of sufficient scale to allow for *large-scale crack-bridging*. The test achieved the following outcomes:

- Produced a large, high strain-rate delamination crack on a predominantly single interface near the mid-plane of the laminate under loading conditions representative of an in-flight impact during take-off or landing;
- Induced delamination initiation and propagation without the use of a pre-crack;
- Avoided any auxiliary failure modes such as fibre-failure near the root;
- Made use of a simple pre-preg specimen design with single-sided taper, manufactured using hand lay-up

406 and autoclave curing with soft-sided vacuum bag tooling and a flat tool surface to minimise manufacturing
407 costs

408 Impact tests showed that the amount of delamination generated varied between tests and that a test velocity of
409 $V_i = 165m/s$ was necessary to achieve full delamination. However, using this target test velocity, the projected
410 2D delaminated area was found to range between $A_d = 64\%$ and $A_d = 100\%$. Variation in the delaminated
411 area of a particular specimen was found to have a significant effect on the tip deflections observed, with more
412 heavily-delaminated specimens exhibiting greater amounts of deflection. Large variations in delaminated area
413 between specimens tested under very similar conditions was attributed to various factors such as environmental
414 conditions (e.g. temperature) or local specimen variations at ply termination locations acting as a driver for
415 delamination.

416 Detailed fractographic analysis of the fracture surfaces of a single specimen was performed to investigate the
417 microscopic nature of the fracture behaviour. By estimating the crack mode-ratio using the tilt of the visible
418 shear cusps, it was determined that the crack mode-ratio was likely changing during crack propagation, from
419 more Mode II behaviour near the root to more mixed-mode behaviour nearer the tip.

420 Inclusion of through-thickness reinforcement – such as Z-pins – in composite structures may significantly
421 affect failure behaviour. The test method developed and validated in this study is suitable for investigating the
422 performance of TTR at sub-structure length scales and under realistic loading conditions. Aside from potentially
423 testing the performance of TTR, the test in its current configuration may be used to assess the behaviour of
424 different material systems (e.g. thermoplastic or 3-D woven composites) and different stacking sequences, or
425 the test configuration may be altered to reproduce failure or behaviour of a different kind. The test designed in
426 this study represents an important step forward to populating the entire aerospace pyramid of testing [24] and
427 establishing a framework for the future virtual testing of composite structures.

428 Acknowledgement

429 The authors wish to acknowledge the support of Rolls-Royce plc through the Composites University Technology
430 Centre (UTC) at the University of Bristol and through the Lightweight Structures and Materials and Robust

Design UTC at the Technische Universität Dresden. The EPSRC is acknowledged through the Centre for Doctoral Training in Composites Manufacture (grant no. EP/L015102/1) as well as the "Understanding Delamination Suppression at High Deformation Rates in Through-Thickness Reinforced Laminated Composites" project (grant no. EP/M015319/1).

References

[1] L. Zhu, N. Li, and P. Childs, "Light-weighting in aerospace component and system design," *Propulsion and Power Research*, vol. 7, pp. 103–119, June 2018.

[2] D. D. Cartié, G. Dell'Anno, E. Poulin, and I. K. Partridge, "3D reinforcement of stiffener-to-skin T-joints by Z-pinning and tufting," *Engineering Fracture Mechanics*, vol. 73, pp. 2532–2540, Nov. 2006.

[3] H. Cui, M. Yasaee, G. Kalwak, A. Pellegrino, I. K. Partridge, S. R. Hallett, G. Allegri, and N. Petrinic, "Bridging mechanisms of through-thickness reinforcement in dynamic mode I&II delamination," *Composites Part A: Applied Science and Manufacturing*, vol. 99, pp. 198–207, Aug. 2017.

[4] S. Heimbs, T. Bergmann, D. Schueler, and N. Toso-Pentecôte, "High velocity impact on preloaded composite plates," *Composite Structures*, vol. 111, pp. 158–168, May 2014.

[5] G. Dell'Anno, J. Treiber, and I. Partridge, "Manufacturing of composite parts reinforced through-thickness by tufting," *Robotics and Computer-Integrated Manufacturing*, vol. 37, pp. 262–272, Feb. 2016.

[6] E. Greenhalgh and M. Hiley, "The assessment of novel materials and processes for the impact tolerant design of stiffened composite aerospace structures," *Composites Part A: Applied Science and Manufacturing*, vol. 34, pp. 151–161, Feb. 2003.

[7] "Standard Test Method for Mode I Interlaminar Fracture Toughness of Unidirectional Fiber-Reinforced Polymer Matrix Composites," tech. rep., ASTM International, West Conshohocken, PA, Mar. 2013.

[8] "Fibre-reinforced plastic composites — Determination of the mode II fracture resistance for unidirectionally reinforced materials using the calibrated end-loaded split (C-ELS) test and an effective crack length approach ," tech. rep., International Organization for Standardization, Geneva, CH, Mar. 2014.

455 [9] "Standard Test Method for Determination of the Mode II Interlaminar Fracture Toughness of Unidirectional
456 Fiber-Reinforced Polymer Matrix Composites," tech. rep., ASTM International, West Conshohocken, PA,
457 Mar. 2019.

458 [10] "Standard Test Method for Mixed Mode I-Mode II Interlaminar Fracture Toughness of Unidirectional Fiber
459 Reinforced Polymer Matrix Composites," tech. rep., ASTM International, West Conshohocken, PA, 2019.

460 [11] I. Partridge and D. Cartie, "Delamination resistant laminates by Z-Fiber® pinning: Part I manufacture and
461 fracture performance," *Composites Part A: Applied Science and Manufacturing*, vol. 36, pp. 55–64, Jan.
462 2005.

463 [12] A. Rezai, D. Cartia, I. Partridge, and P. Irving, "Interlaminar damage resistance of Z-fiber reinforced
464 structural CFRP," in *Proceedings of the 13th European Conference on Composite Materials*, (Beijing,
465 China), 2001.

466 [13] A. M. Yasaee, B. G. Mohamed, C. G. Allegri, and S. R. Hallett, " Delamination resistance of through-
467 thickness reinforced composites," in *Proceedings of the 16th European Conference on Composite Materials*,
468 (Seville, Spain), 2014.

469 [14] K. H. Sayers, "Design and analysis methods for soft-body impact on laminated composite material and
470 metal jet-engine fan-blades," *Fibre Science and Technology*, vol. 8, pp. 173–206, July 1974.

471 [15] "NASA Technical Report: Impact Resistance of Hybrid Composites Fan Blade Materials (NASA CR-
472 134712)," report, Pratt + Whitney Aircraft (for National Aeronautics and Space Administration (NASA)),
473 Washington, D.C., 1974.

474 [16] "NASA Technical Report: Impact Resistance of Composite Fan Blades (NASA CR-134707)," tech. rep.,
475 National Aeronautics and Space Administration (NASA), Washington, D.C., Mar. 1974.

476 [17] A. Mouritz, "Review of z-pinned composite laminates," *Composites Part A: Applied Science and*
477 *Manufacturing*, vol. 38, pp. 2383–2397, Dec. 2007.

478 [18] S. Read, "Test apparatus and method of testing," US Patent 7,845,207, 2010.

479 [19] G. Kalwak, S. Read, M. Jevons, and N. Petrinic, "Investigation of the delamination characteristics of
480 composite specimens with through-thickness reinforcement using an inertia-constrained soft-body beam
481 bend test specimen," in *Proceedings of the 16th European Conference on Composite Materials*, (Seville,
482 Spain), 2014.

[20] J. Hou and C. Ruiz, "Soft body impact on laminated composite materials," *Composites Part A: Applied Science and Manufacturing*, vol. 38, pp. 505–515, Feb. 2007.

[21] S. G. Miller, K. M. Handschuh, M. J. Sinnott, L. W. Kohlman, G. D. Roberts, R. E. Martin, C. R. Ruggeri, and J. M. Pereira, "Materials, Manufacturing, and Test Development of a Composite Fan Blade Leading Edge Subcomponent for Improved Impact Resistance," p. 26, 2015.

[22] "Material Data Sheet: Hexply 8552 Data Sheet," Hexcel Corporation, 2016.

[23] E. Greenhalgh, *Failure Analysis and Fractography of Polymer Composites*. Woodhead Publishing, 2009.

[24] "Military Handbook - MIL-HDBK-17-1F: Composite Materials Handbook, Volume 1 - Polymer Matrix Composites Guidelines for Characterization of Structural Materials," report, U.S. Department of Defense, Maryland, 2002.